Shannon entropy as an indicator of correlation and relativistic effects in confined atoms

Subhasish Saha and Jobin Jose [*]

Department of Physics, Indian Institute of Technology Patna, Bihta 801103, Bihar, India

Relativistic and correlation effects in endohedrally confined atoms ($A@C_{60}$) have been investigated using many-body techniques. The endohedral environment is approximated as an atom trapped in a spherically symmetric Gaussian annular square well model potential. The objective of the work is to present Shannon entropy as an indicator of (i) correlation effects and (ii) relativistic effects in confined atoms. The correlation energy in Be@C_{60} is studied as a function of the depth of the confining potential to give some idea as to how *Shannon's correlation entropy* is sensitive to the minimum location of correlation energy. To see the prominent relativistic effects in the confined atom, *Shannon's relativistic entropy* of the valence subshell of Ba@C_{60} is scrutinized for different confinement parameters. The influence of relativistic and correlation effects on the Shannon entropy of confined atoms is illustrated.

I. INTRODUCTION

The mechanism of insertion of an atom within the fullerene cage is possible by employing "brute force" implantation. Under high pressure and temperature, one of the carbon-carbon bonds of the C_{60} cage is broken and an atom can pass through the transient hole, forming a stable endohedral system [1,2]. Endohedral systems have promising applications in physics and other fields because of the interesting features that are relevant to a broad range of research areas [3–6] including quantum computing [7], medical science [8], superconductivity [9], material science [10,11], etc. The properties of endohedral atoms have been studied theoretically, and these have opened experimental avenues to investigate the electronic structure and dynamics [12,13] in them. For instance, the level ordering and shell filling of endohedral atoms are predicted to be different compared to free atoms [12,14,15]. The electron scattering and photoionization from confined atoms gained wide interest, and has been investigated both theoretically and experimentally (see [16–23], and references therein). A combination of theoretical and experimental investigation is extremely important for a complete understanding of the endohedral systems.

An endohedral system being multielectronic in nature, it is expected that the many-electron correlation effects have a decisive role in the electronic structure and dynamics. Even though the C_{60} confinement lowers the electronic energies, the electrons which have higher overlap with the C_{60} shell are modified preferentially [12,14]. This selective modification can bring one subshell level energetically close to the other, which makes the electron correlation stronger in endohedral atoms in comparison to bare atoms. Also, relativistic effects have governing importance in confined atoms. Among the various synthesized metallofullerenes, La@C_{60} attracted

attention because of the relativistic effects in the electronic structure also [24]. Needless to say, properties of the $A@C_{60}$ are significantly governed by both the relativistic and correlation effects; therefore, it is important to include higher orders of these corrections in the theoretical investigation.

Correlation energy (E^{Corr}), a term coined by Lowdin [25], is one of the useful parameters in the study of bound and excited states. The correlation energy is defined as the difference between the exact ground-state energy and the Hartree-Fock (HF) energy. The exact energy in the definition refers to the experimental energy of the ground-state from a complete measurement. It is well known that the HF limit is always above the exact energy, therefore the inclusion of correlation effects in any theory brings the energy closer to the exact energy. From this perspective, the energy difference between many-body techniques with and without correlation effects can be considered as the correlation energy introduced due to the corrections in the former. The multiconfiguration Dirac-Fock (MCDF) [26] methodology considers the initial-state correlation by admixing the electronic occupation among different relativistic configurations with appropriate weight factors. The MCDF technique plays an important role in relativistic atomic and molecular electronic structure estimates [27–30]. The difference between energy calculated within a single-configuration description of the atom, i.e., Dirac-Fock (DF) [31] and the MCDF can also be treated as the correlation energy of the atomic system: $E^{Corr} = E_{MCDF} - E_{DF}$, where E_{DF} and E_{MCDF} are respectively the atomic energies in the DF and MCDF treatments. The E^{Corr} from the DF and MCDF thus reflects the correlation effects included due to the mixing of relativistic configurations to represent the atomic initial state. Also, the E^{Corr} encodes the augmented correlation effects due to the relativistic splitting of subshells. Likewise, the energy due to the relativistic correction (E^{Rel}) can be viewed as $E^{Rel} = E_{DF} - E_{HF}$, where E_{DF} and E_{HF} are respectively the atomic energies in the single configuration DF and nonrelativistic HF treatments.

----
[*]jobin.jose@iitp.ac.in

It is well reported that the correlation effects play a decisive role in the electronic structure and dynamics of Be, a low-Z element [32,33]. Similarly, the intemeridate-Z element Ba displays rich effects in photoionization parameters due to the relativistic corrections [34–36]. Although these free atoms were widely tested for relativistic and correlation effects, a systematic investigation of these effects in the confined Be and Ba is scanty in the literature. The fact that the Be@C_{60} and Ba@C_{60} have been isolated in experiments [37,38] is just intensifying the need for theoretical investigation of these confined atoms. The primary objective of the present work is to portray the relativistic and correlation effects in confined atoms in terms of Shannon entropy [39]. The motivation behind this objective is the following. The electronic density calculated in a relativistic many-electron correlation method differs from that obtained in the HF or DF limit. Vyboishchikov reported in his works how the electronic densities of spherically confined Be are different in HF and configuration interaction (CI) approaches [40]. Moreover, in the works of Hasoğlu *et al.* [41], an insightful connection between electron density distribution and correlation effects in Be@C_{60} is found. Likewise, the relativistic effects are also making changes in the geometrical distribution of electronic densities [26]. It is well known that the Shannon entropy encodes signatures of electronic localization or delocalization [42]. Shannon entropy is also an alternative, sometimes superior, formalism to the dispersion relation (Heisenberg uncertainty) to represent the delocalization of electronic density [43]. Hence the present work extrapolates the idea of connection between $E^{\text{Corr}}/E^{\text{Rel}}$ and electronic density into the Shannon entropy. There have been multiple attempts in the literature to define correlation and relativistic effects in terms of information entropy [44–46]. In a recent paper, Romera and Dehesa [47] introduced the concept of the Fisher-Shannon information plane as a specific electron correlation measure in two-electron systems. Likewise, complexity measures of electronic density distribution of many-electron atoms in the relativistic and nonrelativistic calculations were contrasted [44]. All these studies indicate that informational entropic measures are being increasingly applied in studying the electronic structure and properties of atoms and molecules. To remedy the glaring omission of entropic studies on confined many-electron atoms, we define, in the present work, the Shannon correlation and relativistic entropies, by which a benchmarking of correlation energy (E^{Corr}) and relativistic energy (E^{Rel}) in terms of information entropy is accomplished in the endohedral atoms.

While looking for the realistic simulation of endohedral atoms, a method that explicitly includes the position of each C atom of the C_{60} with the correct icosahedral (I_{h}) symmetry will be an ideal choice. Therefore, *ab initio* calculations which take care of the symmetry of the C_{60} molecule will be preferred. However, several recent papers have clearly demonstrated that the detailed symmetry does not affect the electronic structure and dynamics of fullerene complexes. For instance, the photoionization cross sections of C_{60} [48], other fullerenes [49], and even carbon onions [50] were calculated by means of time-dependent DFT (accounting for the realistic icosahedral geometry of the fullerenes) and compared successfully with a model approach that assumed a spherical

symmetry of the molecules. Moreover, the experimental photoionization spectrum of Xe@C_{60}^{+} is also in agreement with what is predicted [51] employing a model potential description of the confinement [52,53]. This shows that the model approach was found to provide a very accurate description of the main features of the photoionization spectra. Moreover, this approach was successfully used to compare with experimental and *ab initio* calculation cross sections on elastic and inelastic scattering of electrons from C_{60} [54,55]. Considering the encouraging agreement between the results, we may conclude that the spherical model, despite its extreme simplicity, is surprisingly successful in its qualitative, and even semiquantitative, predictions compared to the far more elaborate *ab initio* calculations. Although the results slightly differ between different model potentials, overall the methodology is giving a realistic representation of the C_{60} environment. Nevertheless, one must look for the best model potentials that can provide quantitative and qualitative agreement with available experimental and *ab initio* level results.

Several model potentials have been employed to represent the effects of C_{60} confinement in literature, such as annular square well (ASW) [12,13,15,56], δ potential [57], attractive Gaussian shell [58], Gaussian annular square well (GASW) [59], power exponential model [60], Woods-Saxon (WS) [41], etc. In the present work, we choose the diffused GASW model potential [42,59], a hybrid of ASW and Gaussian model potentials, to investigate the sensitivity of the Shannon entropy to the relativistic and many-electron correlation effects. In the present work, we have considered that the Be and the Ba atoms are residing at the center of the cage where the energy is expected to be minimum [61]. Furthermore, keeping the endohedral atom at the center of the shell enables us to use the spherical symmetry of the potential, and hence the calculation becomes much simpler. Section II describes the theoretical methods employed in the present work, which is followed by the results and discussion in Sec. III. The work is concluded in Sec. IV.

II. THEORY

The central field Dirac-Coulomb Hamiltonian for the N-electron atomic system, confined by an endohedral cage, is given by

$$H(\vec{r}_1, \vec{r}_2, ..., \vec{r}_N)$$
$$= \sum_{i=1}^{N} \left(c\vec{\alpha}_i \cdot \vec{p}_i + \beta_i mc^2 - \frac{Z}{r_i} + \frac{1}{2} \sum_{i \neq j} \frac{1}{r_{ij}} + V_{\text{con}}(r_i) \right).$$
$$(1)$$

The wave function of the N-electron system $\Psi(J, M)$ can be compactly written in the form of an $N \times N$ Slater determinant [26]. By employing a frozen orbital approximation, the DF equations can be derived using the variational technique [31]. Although the DF method gives a fair estimate of the ground-state and excited-state properties by including relativistic and exchange interactions, the many-electron correlations are not included in the technique. This creates a gap between the exact energy and the DF energy. The initial-state correlation effects are included in the MCDF technique by

treating the N-electron wave function as a linear superposition of Slater determinants. The multiconfigurational wave function of an atom can be written as [26]

$$\Psi(J, M) = \sum_{i=1}^{K} W_i \Phi(\gamma_i J, M), \qquad (2)$$

where J, M are the quantum numbers of the coupled angular momenta of the electrons and γ_i denotes other labels such as for the configurational composition and the angular momentum coupling scheme, which are needed to identify the state [26]. $\{\Phi(\gamma_i J, M)|i = 1, 2, \ldots, K\}$ is a set of orthonormal configuration state functions (CSFs) and the W_i's are expansion coefficients (weight coefficients), which are obtained self consistently. The weight coefficients are constrained by the normalization of probability: $\sum_{i=1}^{N} |W_i|^2 = 1$. Calculations in the optimized level (OL) mode are performed for Be@C_{60}, in which coefficient weights are chosen for a single atomic state function [26]. For the free atomic system, the details of the procedure for obtaining these wave functions are elaborately discussed in the literature [26,31].

To perform the study of relativistic and correlation effects in confined atoms, we have modified the GRASP92 relativistic atomic structure program by adding $V_{con}(r)$ to the regular atomic potential [62]. The individual atomic orbitals of the A@C_{60} are then solved self-consistently, similarly to the case of free atoms [62]. Note that the methodology and codes are applicable only if the atom is situated in the center of the C_{60} shell, i.e., for a spherically symmetric confinement potential and that potential does not depend upon the angle. The widely used confining environment of endohedral systems (A@C_{60}) is the ASW potential, defined as

$$V_{\text{ASW}}(r) = \begin{cases} -U, & r_c - \frac{\Delta}{2} \leqslant r \leqslant r_c + \frac{\Delta}{2} \\ 0, & \text{otherwise}, \end{cases} \qquad (3)$$

where r_c is the mean radius and Δ is the thickness of the C_{60} cage. The ASW potential has unrealistic discontinuity at the shell boundaries; we have, therefore, used an alternative potential that is spatially smeared out, but has compact borders. We employ a parametrically adjustable superposition of the Gaussian and ASW contribution, referred to as the Gaussian annular square well (V_{GASW}) model potential [42,59],

$$V_{\text{GASW}}(r) = \frac{A}{\sqrt{2\pi}\sigma} e^{-((r-r_c)/\sqrt{2}\sigma)^2} + V_{\text{ASW}}(r), \qquad (4)$$

where $A = -3.59$ a.u., standard deviation $\sigma = 1.70$ a.u., $r_c = 6.7$ a.u., and $\Delta = 2.8$ a.u. The values of Gaussian amplitude and V_{ASW} are parametrically adjusted to get the best fit with the potential used by Puska and Nieminen (V_{PN}) [16]. In their work, the energy spectrum of C_{60} is obtained using the local density approximation (LDA) of the density-functional theory (DFT); the formalism accounted for the interaction of 240 electrons of the cage. The above-fitted model potential, $V_{\text{GASW}}(r)$, thus includes an average effect of the electron-electron and electron-proton interactions of the carbon atoms of C_{60} and has the advantage of removing unrealistic discontinuities at the shell boundaries. Moreover, the GASW model belongs to the class of potentials with a nonflat bottom and hence this could properly simulate the C_{60} shell instead of the very often used ASW model potential [63]. Details of
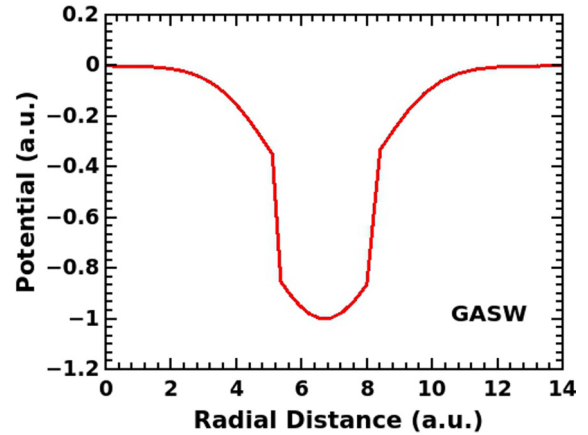
FIG. 1. GASW model potentials for the depth of 1.0 a.u.

the GASW model potential can be found elsewhere [42,59]. Figure 1 shows the GASW model potential for a depth of 1.0 a.u. The smooth, rather than sharp, edge regions of the GASW potential waive any possibility of unphysical effects owing to a discontinuity in the ASW potential.

The difference between energy obtained in the DF and MCDF can be considered as the correlation energy (E^{Corr}) of the A@C_{60}. Likewise, the difference between DF and HF energy (E^{Rel}) can be accepted as a measure of relativistic effect in atoms. The correlation effects of the Be@C_{60} and the relativistic effects of the Ba@C_{60} are studied by varying the depth of the GASW confinement potential. We try to attribute the relativistic and correlation effects to change in the electronic density through the Shannon entropy, which is described below.

Shannon entropy [39] in an atomic system provides in-depth knowledge of electron correlations, the electronic probability density, and especially about the localization of electron density. The radial part of Shannon entropy of the probability density in the position spaces is given by [39]

$$S_r = -\int_{r=0}^{\infty} \rho(r) \ln \rho(r) r^2 dr, \qquad (5)$$

where $\rho(r)$ denotes normalized one electron probability density in position space. Information entropy quantifies the extent of distribution of the probability density in the position space. Bound-state energy and the corresponding position space wave function of the orbital electron of a confined atom are obtained in the present work by solving the central Dirac-Coulomb field equation in the DF and MCDF methodology as described above. To a good approximation, the nonrelativistic HF parameters are obtained by solving the DF equations the *high-c* limit [64].

Due to the relativistic many-electron correlation effects in the initial state, the total electron density can be altered, preserving the normalization conditions. In other words, the change in the electronic probability density and therefore change in the localization properties can be thought of as a signature of relativistic and correlation effects. For example, modifications in the electron density of confined He, Be, and Be^{2+}, reflected in the density moments (μ_n) due to the correlation effects, is illustrated in the work of Vyboishchikov

[40]. Similarly, the DF electrons are more bound than the non-relativistic counterpart; consequently, the DF radial density distribution is more compact than that of HF formalism [26]. Therefore, we can also expect a change in Shannon entropy due to the change in the localization of electronic cloud owing to these effects. An objective of the present work is to look for signatures of relativistic and correlation energies in Shannon's information entropy in confined atoms. For elucidating the change in the Shannon entropy due to the inclusion of correlation and relativistic effects, we define an absolute change in the electronic density between two different methods. In the present work, the change in the electronic probability density between the DF and MCDF is defined as *correlated electron density*: $\rho_{Corr}(r) = |\rho_{MCDF}(r) - \rho_{DF}(r)|$ and that between DF and HF is considered as the change in *electron density due to relativistic effects*: $\rho_{Rel}(r) = |\rho_{DF}(r) - \rho_{HF}(r)|$.

The electronic densities in the MCDF level, $\rho_{MCDF}(r)$, were calculated in a straightforward way employing the weight coefficients and the CSFs obtained in the SCF procedure. The $\rho_{Corr}(r)$ and the $\rho_{Rel}(r)$ represent the incremental change in the electronic density due to correlation and relativistic effects respectively, which also encodes the change in localization due to these effects. Therefore, *Shannon's correlation entropy* measures the degree of localization or diffusion of $\rho_{Corr}(r)$ due to the correlation effects, defined as

$$(S_r)^{Corr} = - \int_{r=0}^{\infty} \rho_{Corr}(r) \ln \rho_{Corr}(r) r^2 dr, \qquad (6)$$

and *Shannon's relativistic entropy* is a measure of relativistic effects, given as

$$(S_r)^{Rel} = - \int_{r=0}^{\infty} \rho_{Rel}(r) \ln \rho_{Rel}(r) r^2 dr. \qquad (7)$$

The present work aims to bring a connection between $(S_r)^{Corr}$ and E^{Corr} in the confined Be atom and $(S_r)^{Rel}$ and E^{Rel} in the confined Ba atom using the GASW confinement model.

III. RESULTS AND DISCUSSION

A. Correlation effects in Be@C$_{60}$

The ground state of Be@C$_{60}$ in the DF approach is represented by a single configuration, $1s^2 2s^2$. It is well known that the interaction between $1s^2 2s^2$ and $1s^2 2p^2$ configurations contributes the most to the initial-state correlation effects in a free Be atom [41,65]. However, this may not be true for confined Be@C$_{60}$. Therefore, the MCDF initial state of the confined Be is obtained by allowing the two-electron excitations to the low-lying bound orbitals $2p_{1/2}$, $2p_{3/2}$, and $3s$. The two-electron excitations are selectively included and thereby two separate multiconfigurational initial states are considered for contrasting the correlation effects in Be@C$_{60}$: (1) $1s^2\{2s^2 + 2p_{1/2}{}^2 + 2p_{3/2}{}^2\}$, $J = 0$, and (2) $1s^2\{2s^2 + 2p_{1/2}{}^2 + 2p_{3/2}{}^2 + 3s^2\}$, $J = 0$; the former configuration is denoted as configuration 1 (C$_1$) and the latter as configuration 2 (C$_2$) in this work. Comparison of correlation energy from the calculations employing C$_1$ and C$_2$ configurations will showcase the contribution of $3s$ subshells in a confined atom. This will also test whether the configuration interaction is similar in free Be and Be@C$_{60}$.
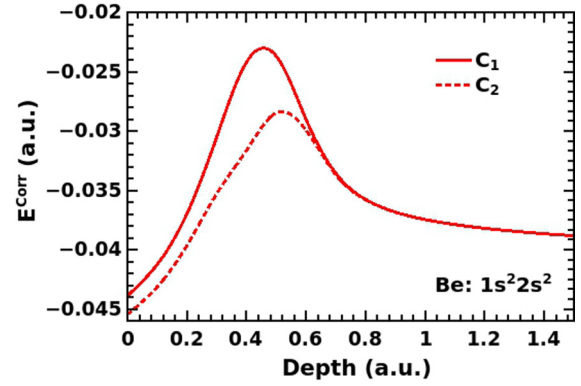
FIG. 2. Correlation energy of confined Be as a function of well depth.

Using the configuration interaction (CI) terms in the MCDF wave function, the total energies and subshell thresholds of confined Be were calculated for a range of potential depths starting from free case to $V_{con}(r_c) = 1.5$ a.u. The DF energies were also computed in the confining potential for the same range of depths. The total energies of the free Be in the MCDF calculations employing C$_1$ and C$_2$ configurations are -14.6197 a.u. and -14.6212 a.u., whereas the same in the single configuration DF formalism is -14.5759 a.u.; the difference of DF and MCDF energies signify the correlation correction. Note that the energy is slightly different from the MCHF result [41], which is -14.6659 a.u. from a CI expansion including 52 configurations [65]. The total energy of Be@C$_{60}$ from the C$_2$ configuration calculation is slightly higher in magnitude compared to C$_1$ calculation, which indicates that the correlation effects are increased with the addition of more CI terms, which is natural to expect. The insignificant difference in the total energies in the C$_1$ and C$_2$ calculation indicates that the $3s$ orbitals play less role in contributing to the realistic ground state of free Be. Nevertheless, this claim may not be true for Be@C$_{60}$, which will be scrutinized in the present work.

It is of special interest to know the evolution of correlation energy, $E^{Corr} = E_{MCDF} - E_{DF}$, as a function of well depth of the model potential, which is shown in Fig. 2. Although the E^{Corr} from the C$_1$ and C$_2$ configuration calculations are qualitatively similar, it is quantitatively increased for C$_2$ as expected; the difference is apparent for intermediate confinement depths considered. Starting from the free Be, the magnitude of correlation energy becomes smaller as the depth of the confining potential increases up to a certain well depth ($\sim$0.44 a.u. for C$_1$ and $\sim$0.52 a.u. for C$_2$), and then increases as the strength of the well increases further. It needs to be emphasized that the peak in the E^{Corr} represents a minimum of the correlation energy. The minimum location of the correlation energy is shifted slightly to the deeper well side in the C$_2$ calculation, which is evidently due to the admixing of the additional configuration $1s^2 3s^2$ with the terms in C$_1$ configuration. Moreover, up to a well depth of $\sim$0.7 a.u., the magnitude of the correlation energy in the C$_2$ calculation is larger compared to that in the C$_1$ calculation, with the difference being largest at the peak position of the correlation energy. Beyond the well depth $\sim$0.7 a.u., the correlation
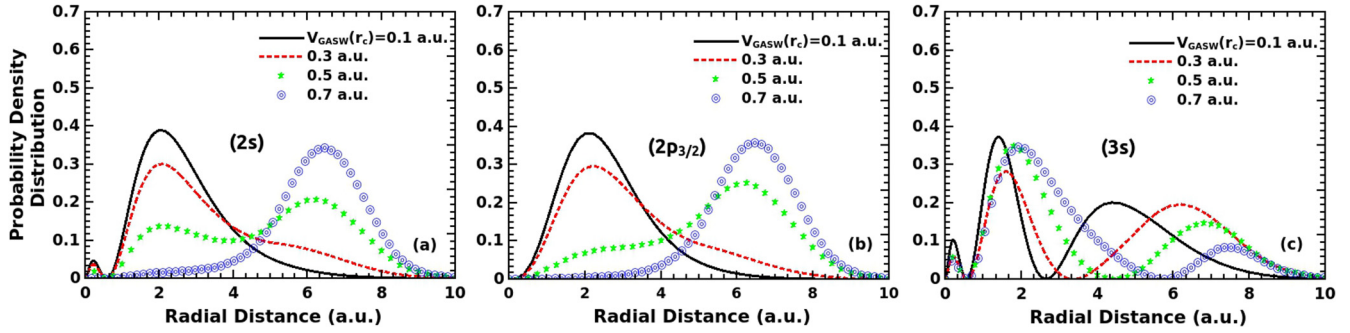
FIG. 3. Position probability density distribution of $2s$ (left), $2p$ (middle), and $3s$ (right) one-electron orbitals in Be@C_{60} for a selection of well depths of model potential using the C_2 configuration.

energy in the C_1 and C_2 calculation becomes identical. This trend of E^{Corr} means that the effect of the configuration $1s^2\,3s^2$ is significant only for Be@C_{60} with intermediate confinement depths. The present analysis, hence, shows that the configurations in the C_1 calculation adequately represents the initial state of free Be, but additional configurations are required for confined Be.

To understand the behavior of E^{Corr}, we first trace out the variation of the position probability density distribution of the spectroscopic $2s$, correlation $2p_{3/2}$, and $3s$ one-electron orbitals for a selection of well depths, which is shown in Fig. 3. Note that the orbitals from the C_2 configuration calculation are plotted in Fig. 3; the trend of variation of $2s$ and $2p$ orbitals is identical to that from the C_1 configuration calculation. The $2p_{1/2}$ electronic density (not shown) is not different from that of $2p_{3/2}$ because spin-orbit forces are less dominant for confined Be. At first, the evolution of electronic density from the C_1 calculation is investigated. Up to the depth $V_{con}(r_c) = 0.3$ a.u., the electronic probability density of both $2s$ and $2p$ orbitals are mostly distributed close to the nuclear region, beyond which both the density distributions are seen comoving towards the C_{60} shell region [Figs. 3(a) and 3(b)]. This behavior is quite opposite to that of $1s$ and $2s$ probability densities of H@C_{60}, where the orbitals are shifted in opposite directions when the confinement strength is increased; the $1s$ electron density is shifted to the C_{60} shell region, whereas the density of the $2s$ electron is moved to the nuclear side [42]. This behavior in H@C_{60} is attributed to the avoided level crossing between orbitals of the same symmetry, famously known as the von Neumann–Wigner noncrossing rule [56,66]. In the Be@C_{60} case, since the ground and excited states have different symmetries, they don't repel each other, rather they are seen moving together. When $V_{GASW}(r_c)$ reaches ~ 0.7 a.u., both the electronic density of $2s$ and $2p$ radial orbitals are predominantly sucked by the C_{60} shell.

We investigate next the evolution of $3s$ probability density distribution [Fig. 3(c)] as the confinement depth is varied. For the free case, the probability amplitude of the $3s$ state spans over a wide range of radial distance, with significant contribution near the nuclear side. When the well depth is 0.4 a.u., the $3s$ position space wave function is equally distributed over the nuclear and well region; the electron density is highly delocalized. This posture of $3s$ electron density is akin to the behavior of $2s$ and $2p$ electrons. As depth increases further up to depth 0.7 a.u., the $3s$ position space wave function is

transferred from the confinement region to the inner Coulombic region. The evolution of orbitals of C_1 configuration is quite contrary to that of the $3s$ orbital. There exists a competition between the gain of the population of $3s$ electron and loss of $2s$ and $2p$ electrons in the atomic region. A reverse competition is exhibited in the confinement region also. It is noteworthy that this competition is absent in the C_1 calculation. Thus, the minimum location of the correlation energy is slightly shifted to the deeper well side for the case of C_2 due to this competition and the associated correlation effect.

The correlation energy (Fig. 2) and the delocalization of electronic cloud of the Be@C_{60} are intrinsically connected, which was shown in the work of Hasoğlu *et al.* [41]. According to their work, more delocalized $2s$ and $2p$ orbital electrons tend to occupy a larger radial space, which causes the $2s$ and $2p$ orbital electrons to be further apart, thereby contribution of the interaction term $(1/|r_{ij}|)$ reduces. The delocalization of $2s$ and $2p$ electrons, thus, is responsible for the minimum in the correlation energy. In our calculations, the minimum of E^{Corr} happens at ~ 0.44 a.u. for C_1 and it is at this depth the $2s$, $2p_{1/2}$, and $2p_{3/2}$ electrons have almost equal probabilities in the atomic well region and C_{60} shell region. On the contrary, on both sides of the minimum location of E^{Corr}, the $2s$ and $2p$ electrons occupy a smaller range of volume at extremely high and low confinement depths, which is why the electron-electron interaction and thereby the correlation effects are enhanced. A similar explanation can be given for the nature of the E^{Corr} curve in the C_2 calculation. The peak happens at ~ 0.52 a.u. of well depth in the C_2 configuration calculation. It is at this depth the $3s$ electrons are highly delocalized, with similar delocalization features for $2s$ and $2p$ electrons. Hence the electron densities of $2s$, $2p$, and $3p$ subshells are overlapped in a wider region, which reduces the interaction term $(1/|r_{ij}|)$ and consequently a minimum correlation energy.

It is well known that the information entropies do carry signatures of the spread of probability density [42]. The information entropies like Shannon entropy, Fisher entropy, etc., have been instrumental in predicting electronic structure properties, including correlation effects [67–71]. Having understood the agreement between the delocalization of electronic densities and correlation effects, we aim to discover an insightful connection between correlation energy and Shannon entropy. For accomplishing the same, the radial part of Shannon correlation entropy in position space $(S_r)^{Corr}$ is
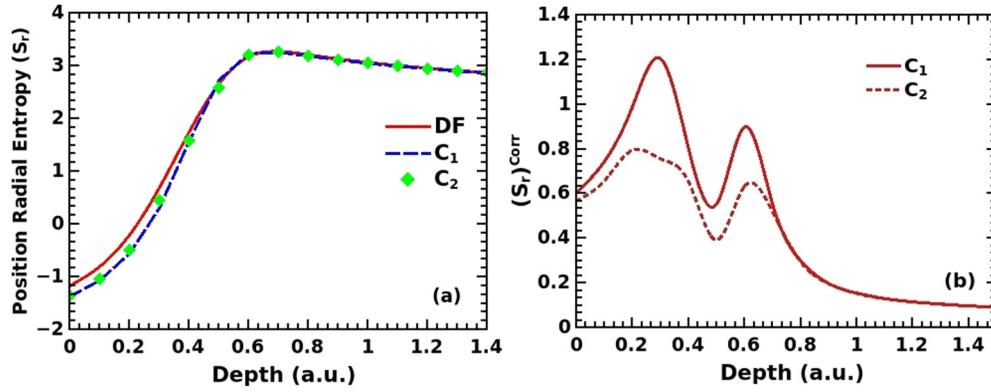
FIG. 4. Radial part of (a) Shannon entropy in position space and (b) correlation entropy of confined Be as a function of confinement well depth.

defined in Eq. (3), employing $\rho_{\text{Corr}}(r)$. The $\rho_{\text{Corr}}(r)$ represents the incremental change in the electronic densities due to correlation effects, which also signifies delocalization in electron density due to the correlation effects. Therefore, the $(S_r)^{\text{Corr}}$ is expected to convey meaningful information regarding the change in electron density due to the correlation effects.

The evolution of position radial Shannon entropy and the correlation entropy as a function of well depth is shown in Fig. 4 in C_1 and C_2 configuration calculations. With the increase in depth of the confinement potential, the position radial Shannon entropy is also seen increased, exhibiting a similar trend as that of the delocalization of electrons; the trend is uniform in both C_1 and C_2 calculations. At depth $\sim$0.44 a.u., the DF and the MCDF position radial entropies intersect with each other for the case of C_1, where the correlation energy is minimum, i.e., at this depth the MCDF density distribution tends to that of DF. The crossing of MCDF and DF entropies in the C_2 configuration happens at depth $\sim$0.52 a.u., where the minimum location of the correlation energy is also located. At the minimum correlation energy point, the electronic density of correlated Be@C_{60} is represented predominantly by the $2s$ electrons, which is reflected from the intersection of position Shannon entropies from DF and MCDF approaches. As the confinement potential is increased further from 0.44 to 1.0 a.u., position space wave function shifts towards the shell region and the separation between MCDF and DF entropies widens, i.e., correlation energy increases. The position radial Shannon entropy (S_r) attains its maximum value at $\sim$0.6 a.u. depth of confining potential, indicating that the $2s$ and $2p$ electrons are now well states. With further increase of potential depth, a gradual decrease in the position radial entropy is seen, which hints that the $2s$ and the $2p$ electrons are getting more and more localized in the confining well; an increase in correlation energy will be the consequence.

The Shannon entropy does not exhibit any specific features of minimum correlation energy at $\sim$0.44 a.u. for C_1 ($\sim$0.52 a.u. for C_2) in the form of a maximum or minimum. The Shannon correlation entropy $(S_r)^{\text{Corr}}$ in Fig. 4(b), on the other hand, shows a surprising similarity with the correlation energy graph shown in Fig. 2 that there exists a minimum at depth $\sim$0.44 a.u. in the C_1 calculation, which is corresponding to the peak in the E^{Corr}; the peak in E^{Corr} indicated the

minimum correlation energy. Similarly, a global minimum is exhibited in the $(S_r)^{\text{Corr}}$ in the C_2 calculation at well depth $\sim$0.52 a.u., which is where the minimum correlation energy is seen. First, we analyze the correlation entropy from the C_1 calculation. Incidentally, two maxima have been seen (at confinement depth $\sim$0.3 a.u. and $\sim$0.6 a.u.) around the minimum location of the $(S_r)^{\text{Corr}}$ in the case of the C_1 calculation. This indicates that the changes in the electron density $[\rho_{\text{Corr}}(r)]$ due to the correlation effects are delocalized most at these depths; the C_{60} state and the atomic state contribute to the additional electron densities due to correlation effects at these well depths. This claim is verified from the analysis of correlated electron density $\rho_{\text{Corr}}(r)$ (figure not presented). For the free case, the correlation density $\rho_{\text{Corr}}(r)$ is mostly contributed by the atomic state and least by the shell state. On the contrary, at depths $\sim$0.3 and $\sim$0.6 a.u. an equal contribution to correlation density from the atomic state and shell state occurs. This implies the maximum spreading of $\rho_{\text{Corr}}(r)$ and consequent peaks in the correlation entropy. The Shannon correlation entropy is quite a meaningful quantity as it is an indicator of dissimilarity in the electron density of DF and MCDF formalism due to correlation effects. In the confined Be, the spread of the correlated electron density is minimum at the minimum of correlation energy, which is reflected as the minimum in the $(S_r)^{\text{Corr}}$ graph. This is quite expected as the $2p$ orbitals are least contributing at this point; MCDF and DF densities tend to be alike.

A slightly different qualitative nature is seen in the correlation entropy curve from the C_2 calculations; a local shallow minimum is exhibited at $\sim$0.3 a.u., which makes a broader maximum compared to that in the C_1 calculation. The shallow minimum embodies as a shoulderlike structure in the $(S_r)^{\text{Corr}}$. The differences in the C_2 calculation are indicative of the competition between $1s^2 3s^2$, $1s^2 2p^2$, and $1s^2 2s^2$ configurations. In short, the $(S_r)^{\text{Corr}}$ reflects the incremental changes in the electron densities due to the correlation effects. Moreover, the signature of contribution from different configurations is also evident. A global minimum at well depth 0.52 a.u. in the correlation entropy is indicative of the minimum correlation energy in the system. Hence, a detailed analysis of the $(S_r)^{\text{Corr}}$ reveals rich information regarding changes due to the correlation effects in the electron densities, its localization properties, weightage of different configuration, etc.
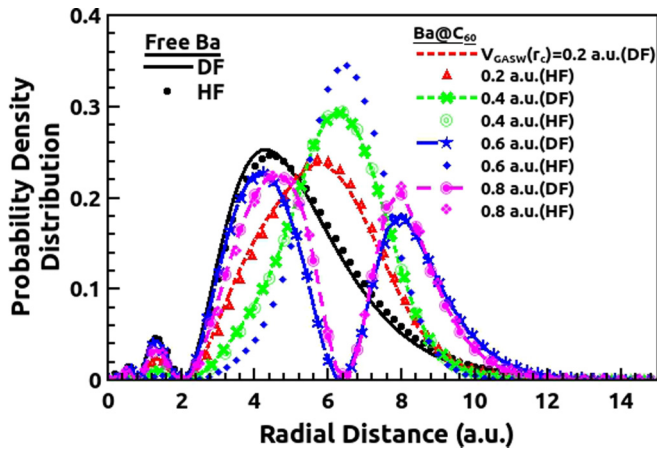
FIG. 5. Position probability density distribution of $6s$ one-electron orbitals in Ba@C_{60} for a selection of well depths of model potential.

B. Relativistic effects in Ba@C_{60}

In the case of confined Ba, the effect of relativity on the Shannon entropy of valence subshell, $6s$, is investigated as it has larger overlap with the GASW. In particular, the focus is on the systematic variation of relativistic Shannon entropy as the confinement depth is altered. To illustrate the contrasting delocalization properties of Ba@C_{60} in HF and DF formalism, Fig. 5 shows the probability density distribution of the $6s$ orbital with varying confinement depths. One can notice that the DF electronic densities are more compact compared to the nonrelativistic counterpart owing to the increased binding energy of the relativistic orbitals. For the free case, the DF and HF orbitals lie predominantly inside the C_{60}.

As the strength of confinement is increased, the orbital is mixed with a wave function localized in the confining well, i.e., "hybridization" results from this superposition. It is noteworthy that the $6s$ orbital of Ba@C_{60} gains an extra node at a well depth of 0.6 a.u. in DF and at 0.8 a.u. in the HF formalism. It is well known that the orbitals of C_{60} are commonly classified as σ or π according to whether they have zero or one radial node located near the carbon cage [55]. Thus, the present calculations are suggestive of the fact that the Ba orbital is hybridized with the π orbital of the C_{60} leading to a node in the probability density on the C_{60} shell. This observation is further supported by conclusion of combined experimental and theoretical electronic structure studies of Ba@C_{60}, that the Ba atoms can hybridize strongly with the π-type functions of the C_{60} [72]. A similar feature is exhibited in the density-functional theory studies of Xe@C_{60}, where powerful hybridization of the Xe $5s$ subshell with C_{60} π function is reported, leading to a node in the electronic density within the shell region [73]. It is worth mentioning that despite the use of simplified model C_{60} confinement potentials, the present calculations realistically encode the hybridization properties of Ba@C_{60} very similar to an *ab initio* level calculation. Furthermore, the present work infers that the nodal behavior of confined atom orbitals could be different from that of hydrogenic orbitals.

In addition to the compactness of the DF orbitals, the hybridization properties of Ba orbitals are also sensitive to the relativistic effects. While the hybridization of DF orbitals happens at 0.6 a.u. of well depth, it requires additional well depth for the similar hybridization to occur in HF calculations. This could be due to the altered screening potential that the HF and DF electron sees as it moves from the atom side to the well side upon changing the well depth. This is suggestive of the fact that the relativistic effect changes the localization properties of $6s$ orbitals since the hybridization is sensitive to it. Furthermore, one may expect enhanced E^{Rel} for those confinement depths, at which hybridization happens.

From the perspective of geometrical changes to the electron density due to the relativistic effects, Fig. 6 shows the ground-state properties of Ba@C_{60} $6s$ orbital as function of well depth. The $6s$ binding energy [Fig. 6(a)] shows considerable differences in the HF and DF formalisms; the energies increase gradually as the confinement depth is increased up to 0.5 a.u. in the DF and 0.7 a.u. in the HF methodology. In this region, the $6s$ electrons are moving from the atomic side to the well side. This is marked by a gradual increase in the Shannon entropy [Fig. 6(c)], which indicates the enhanced delocalization and therefore disorder consequent to the drift of electrons to the fullerene side. The Shannon entropy becomes stabilized as the electrons are shifted to the well side, but maintaining the same nodal behavior as that of free atoms. The strong hybridization with the π orbital is marked by a sudden drop in the binding energy of the $6s$ orbital at 0.6 a.u. of well depth in DF and at 0.8 a.u. in the HF case. It is as if the Coulomb repulsion with the fullerene electrons has made the Ba $6s$ orbital less bound. This observation is much akin to the less bound hybridized orbital in the Xe@C_{60} case [73]. The additional node of hybridized Ba $6s$ orbital is indicated by the sudden increment in the Shannon entropy from 0.4 to 0.6 a.u. of well depth in DF and 0.6 to 0.8 a.u. in HF. This is consequent to the increased delocalization due to the bimodal distribution of electron density within the C_{60} shell. Note that the Shannon entropies of the DF and HF orbitals are largely different in this region. With further increases in the well depth the binding energy increases and the Shannon entropy gradually decreases. This means that the hybridized $6s$ electrons are getting more and more compact within the shell region.

Of particular interest is the E^{Rel} [Fig. 6(b)] and $(S_r)^{Rel}$ [Fig. 6(d)] as the confinement depth is varied, which is indicative of the changes in the binding energies and electronic density distribution respectively due to the relativistic effect. One may note that E^{Rel} and $(S_r)^{Rel}$ show identical qualitative features upon variation of confinement depth. For instance, the disorder of the system and the energy change due to the relativistic effect are quite small when the strength of the confinement is very low. The only small difference could be due to the more bound nature of the DF orbitals compared to HF, which makes the former less entropic up to a depth of 0.4 a.u. But when the strength of confinement is high enough to transfer the electron from the atomic region to the well region, then the dynamics is completely different. The E^{Rel} and $(S_r)^{Rel}$ attain a maximum at ∼0.64 a.u. of well depth, which is the hybridization region. At this point, the relativistic effect is so strong that there exists high complexity in the DF orbitals
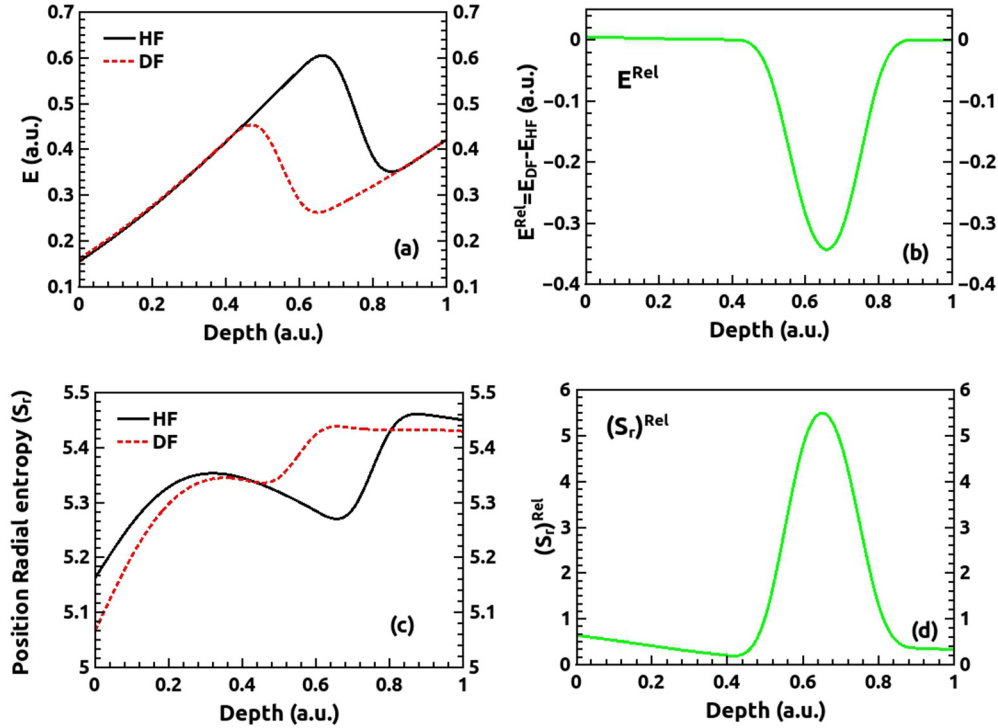
FIG. 6. Properties of $6s$ orbital of Ba@C$_{60}$ as a function of the C$_{60}$ well depth: (a) DF and HF energies, (b) E^{Rel}, (c) radial part of Shannon entropy in position space, and (d) relativistic Shannon's entropy.

compared to that of HF. This means that the relativistic effects are mostly due to the changes in the hybridization in Ba@C$_{60}$. The enhanced $(S_r)^{\text{Rel}}$ indicates that the delocalization due to the relativistic effect is owing to the sensitivity of DF and HF orbitals to the hybridization properties. After the depth 0.8 a.u., E^{Rel} and $(S_r)^{\text{Rel}}$ maintains a low value as in the case of low confinement depths. In this region also, the major effect of relativity is to compactify the $6s$ orbitals by making them more bound compared to HF. Consequently, the DF orbitals will be less entropic.

The Shannon entropy, in the present context, is a measure of the delocalization or the lack of structure in the electronic probability distribution of confined atoms. It is well known that information entropic measures provide evidence of correlation and relativistic effects [44,74]. The present work belongs to the same category which tries to identify features of Shannon entropy with reference to the geometrical changes in electronic density in endohedrals due to the relativistic and correlation effects. At this point, it will be worth discussing the scope for measurable quantities of endohedrals in an experiment to verify the predictions employing the information entropic quantities. A possibility of measurement of information entropy, in particular Shannon entropy, could be only realized if electron density can be measured. Hayman *et al.* have shown that the average electron density is a measurable quantity from the x-ray-scattering studies [75]. According to the work of Hayman *et al.* [75], the average electron density $\langle \rho \rangle$ of an atom is intrinsically connected to the scattered x-ray intensity. Along similar lines, a result connecting x-ray-scattering and average electron densities was derived by Stewart *et al.* [76]. These works hint that the average entropy of an atom could, in principle be measured in an

x-ray-scattering experiment. With the unprecedented advancements in the spectroscopy field, it is quite possible to accomplish x-ray scattering from confined systems [77]. An impetus to the experimental realization from confined atoms is already in place after the photoionization experiments with Xe@C$^+_{60}$ [52,53]. This suggests that the Shannon entropy of endohedrals can be measured which will carry information related to relativistic and correlation effects; for instance, the altered Shannon entropy owing to the sensitivity of hybridization of confined atom to the relativistic effects could be measured.

IV. CONCLUSION

The present work attempts to draw a connection between delocalization properties of atomic electrons and relativistic or correlation effects employing Shannon information entropy in a confined atom, Ba@C$_{60}$/Be@C$_{60}$. Correlation and relativistic entropies have been defined, which carry the information of relativistic many-electron correlation effects; a global minimum is exhibited by the $(S_r)^{\text{Corr}}$ at the minimum location of correlation energy and a maximum in the $(S_r)^{\text{Rel}}$ at the location of peak of the relativistic energy. Other features of the $(S_r)^{\text{Rel}}$ or $(S_r)^{\text{Corr}}$ such as local minimum and maximum unveiled the delocalization properties of $\rho_{\text{Rel}}(r)$ or $\rho_{\text{Corr}}(r)$, which represents the incremental change in the electron probability density due to the relativistic or correlation effects.

Two separate configurational states, C$_1$($1s^2\{2s^2 + 2p_{1/2}{}^2 + 2p_{3/2}{}^2\}$) and C$_2$($1s^2\{2s^2 + 2p_{1/2}{}^2 + 2p_{3/2}{}^2 + 3s^2\}$), are considered to show the effects of correlation in Be@C$_{60}$ as the confinement depth is varied. There is a small window of depth, in which the $1s^2 \, 3s^2$ configuration plays a major role

in the correlation effects in Be@C_{60}. The minimum location of the correlation energy is shifted to the deeper well side in the C_2 calculation due to the admixing of the additional configuration $1s^2\,3s^2$ with the terms in C_1; minimum correlation energy in C_1 and C_2 configuration calculation are respectively at 0.44 and 0.52 a.u. of confinement depth. The features of the correlation energy variation are rightly reflected in the correlation entropy; the $(S_r)^{Corr}$ exhibited a global minimum at the location of the minimum correlation energy. The $2s$, $2p_{1/2}$, $2p_{3/2}$, and $3s$ electrons have almost equal probabilities in the atomic well region and the C_{60} shell region at the location of minimum correlation energy, and therefore almost the same delocalization properties. The similar electronic probability spread signifies an enhanced overlap between them reducing the *e-e* interaction and consequently a minimum in the E^{Corr} and $(S_r)^{Corr}$.

The delocalization properties of electrons in confined atom and the impact of relativistic effects are intrinsically connected. The DF electrons are less entropic than the HF electrons. In addition, the present work demonstrated that the relativistic effects are enhanced in the Ba@C_{60} compared to free Ba; relativistic effects predominantly affect the hybridization of atomic orbitals with the C_{60} states. For sufficiently high depths, the electronic densities are completely transferred to the C_{60} side due to hybridization, acquiring a bimodal electronic distribution within the shell region. As a result, the Shannon entropy and the $(S_r)^{Rel}$ increases, which in turn maximizes the E^{Rel}.

A major highlight of the present work is the insightful connection between the relativistic or correlation energy and the Shannon entropy, from the perspective of differences in the electron density due to these effects. This work illustrates and provides evidence that the entropic information may be used as a relativistic and correlation measure, and this could influence the measurable characteristic of A@C_{60}.

ACKNOWLEDGMENT

[1] M. Saunders, H. A. Jiménez-Vázquez, R. J. Cross, and R. J. Poreda, Science **259**, 1428 (1993).

[2] R. L. Murry and G. E. Scuseria, Science **263**, 791 (1994).

[3] H. Shinohara, Rep. Prog. Phys. **63**, 843 (2000).

[4] A. L. Buchachenko, J. Phys. Chem. B **105**, 5839 (2001).

[5] L. Forró and L. Mihály, Rep. Prog. Phys. **64**, 649 (2001).

[6] P. Moriarty, Rep. Prog. Phys. **64**, 297 (2001).

[7] W. Harneit, C. Boehme, S. Schaefer, K. Huebener, K. Fostiropoulos, and K. Lips, Phys. Rev. Lett. **98**, 216601 (2007).

[8] J. B. Melanko, M. E. Pearce, and A. K. Salem, in *Nanotechnology in Drug Delivery*, edited by M. M. de Villiers, P. Aramwit, and G. S. Kwon (Springer, New York, 2009), p.105.

[9] R. H. Zadik, Y. Takabayashi, G. Klupp, R. H. Colman, A. Y. Ganin, A. Potočnik, P. Jeglič *et al.*, Sci. Adv. **1**, e1500059 (2015).

[10] R. B. Ross, C. M. Cardona, D. M.Guldi, S. G. Sankaranarayanan, M. O. Reese, N. Kopidakis, J. Peet, B. Walker, G. C.Bazan, E. V. Keuren, B. C. Holloway, and M. Drees, Nat. Mater. **8**, 208 (2009).

[11] J. F. Nierengarten, New J. Chem. **28**, 1177 (2004).

[12] V. K. Dolmatov, A. S. Baltenkov, J. P. Connerade, and S. T. Manson, Radiat. Phys. Chem. **70**, 417 (2004), and references therein.

[13] V. K. Dolmatov, in *Advances in Quantum Chemistry: Theory of Quantum Confined Systems*, edited by J. R. Sabin and E. Brandas (Academic, New York, 2009), p.13, and references therein.

[14] J. P. Connerade, V. K. Dolmatov, and P. A. Lakshmi, J. Phys. B: At., Mol. Opt. Phys. **33**, 251 (2000).

[15] J. P. Connerade, V. K. Dolmatov, P. A. Lakshmi, and S. T. Manson, J. Phys. B: At., Mol. Opt. Phys. **32**, L239 (1999).

[16] M. J. Puska and R. M. Nieminen, Phys. Rev. A **47**, 1181 (1993).

[17] A. S. Baltenkov, J. Phys. B: At., Mol. Opt. Phys. **32**, 2745 (1999).

[18] M. Ya. Amusia, A. S. Baltenkov, and U. Becker, Phys. Rev. A **62**, 012701 (2000).

[19] M. A. McCune, E. M. Mohamed, and H. S. Chakraborty, Phys. Rev. A **80**, 011201(R) (2009).

[20] V. K. Dolmatov, P. Brewer, and S. T. Manson, Phys. Rev. A **78**, 013415 (2008).

[21] V. K. Dolmatov, M. Y. Amusia, and L. V. Chernysheva, Phys. Rev. A **88**, 042706 (2013).

[22] V. K. Dolmatov, M. Y. Amusia, and L. V. Chernysheva, Phys. Rev. A **90**, 032717 (2014).

[23] V. K. Dolmatov, M. Y. Amusia, and L. V. Chernysheva, Phys. Rev. A **95**, 012709 (2017).

[24] J. P. Connerade and R. Semaoune, J. Phys. B: At. Mol. Opt. Phys. **33**, 869 (2000).

[25] P. O. Löwdin, Phys. Rev. **97**, 1509 (1955).

[26] I. P. Grant, *Relativistic Quantum Theory of Atoms and Molecules, Theory and Computation* (Springer-Verlag, New York, 2007).

[27] O. Gorceix, P. Indelicato, and J. P. Desclaux, J. Phys. B: At. Mol. Opt. Phys. **20**, 639 (1987).

[28] M. H. Chen, K. T. Cheng, and W. R. Johnson, Phys. Rev. A **47**, 3692 (1993).

[29] J. Hata and I. P. Grant, J. Phys. B: At. Mol. Opt. Phys. **14**, 2111 (1981).

[30] P. Indelicato, Phys. Rev. Lett. **77**, 3323 (1996).

[31] W. R. Johnson, *Atomic Structure Theory, Lectures on Atomic Physics* (Springer, New York, 2007).

[32] J. J. Omiste, W. Li, and L. B. Madsen, Phys. Rev. A **95**, 053422 (2017).

[33] V. Radojević and W. R. Johnson, Phys. Rev. A **31**, 2991 (1985).

[34] V. Radojević, M. Kutzner, and H. P. Kelly, Phys. Rev. A **40**, 727 (1989).

[35] A. Ganesan, P. C. Deshmukh, A. S. Kheifets, V. K. Dolmatov, and S. T. Manson, J. Phys.: Conf. Ser. **875**, 022021 (2017).

[36] M. Kutzner, G. P. Wright, and G. B. Cross, Phys. Rev. A **71**, 064702 (2005).

[37] T. Ohtsuki, K. Masumoto, K. Ohno, Y. Maruyma, Y. Kawazoe, K. Sueki, and K. Kikuchi, Phys. Rev. Lett. **77**, 3522 (1996).

[38] Y. Kubozono *et al.*, J. Am. Chem. Soc. **118**, 6998 (1996).

[39] C. E. Shannon, Bell Syst. Tech. J. **27**, 379 (1948).

[40] S. F. Vyboishchikov, J. Comput. Chem. **37**, 2677 (2016).

[41] M. F. Hasoğlu, H.-L. Zhou, and S. T. Manson, Phys. Rev. A **93**, 022512 (2016).

[42] S. Saha and J. Jose, Int. J. Quantum Chem. **120**, e26374 (2020).

[43] I. Białynicki-Birula and J. Mycielski, Commun. Math. Phys. **44**, 129 (1975).

[44] A. Borgoo, F. De Proft, P. Geerlings, and K. D. Sen, Chem. Phys. Lett. **444**, 186 (2007).

[45] A. Borgoo, P. Geerlings, and K. D. Sen, Phys. Lett. A **372**, 5106 (2008).

[46] T. Yamano, Chem. Phys. Lett. **731**, 136618 (2019).

[47] E. Romera and J. S. Dehesa, J. Chem. Phys. **120**, 8906 (2004).

[48] A. V. Verkhovtsev, A. V. Korol, and A. V. Solov'yov, Phys. Rev. A **88**, 043201 (2013).

[49] A. V. Verkhovtsev, A. V. Korol, and A. V. Solov'yov, J. Phys.: Conf. Ser. **490**, 012159 (2014).

[50] A. Verkhovtsev, A. V. Korol, and A V. Solov'yov, Eur. Phys. J. D **70**, 221 (2016).

[51] M. Y. Amusia, A. S. Baltenkov, L. V. Chernysheva, Z. Felfli, and A. Z. Msezane, J. Phys. B: At. Mol. Opt. Phys. **38**, L169 (2005).

[52] A. L. D. Kilcoyne *et al.*, Phys. Rev. Lett. **105**, 213001 (2010).

[53] R. A. Phaneuf *et al.*, Phys. Rev. A **88**, 053402 (2013).

[54] P. Bolognesi, L. Avaldi, A. Ruocco, A. Verkhovtsev, A.V. Korol, and A. V. Solov'yov, Eur. Phys. J. D **66**, 254 (2012).

[55] C. Winstead and V. McKoy, Phys. Rev. A **73**, 012711 (2006).

[56] L. D. Landau and E. M. Lifshitz, *Quantum Mechanics: Nonrelativistic Theory* (Oxford, Pergamon, 1965).

[57] M. Ya. Amusia, L. V. Chernysheva, and V. K. Dolmatov, Phys. Rev. A **84**, 063201 (2011).

[58] E. M. Nascimento, F. V. Prudente, M. N. Guimarães, and A. M. Maniero, J. Phys. B: At., Mol. Opt. Phys. **44**, 015003 (2011).

[59] S. Saha, A. Thuppilakkadan, H. R. Varma, and J. Jose, J. Phys. B: At. Mol. Opt. Phys. **52**, 145001 (2019).

[60] C. Y. Lin and Y. K. Ho, J. Phys. B: At., Mol. Opt. Phys. **45**, 145001 (2012).

[61] J. Lu, Y. Zhou, X. Zhang, and X. Zhao, Chem. Phys. Lett. **352**, 8 (2002).

[62] F. A. Parpia, C. F. Fischer, and I. P. Grant, Comput. Phys. Commun. **94**, 249 (1996).

[63] M. Ya. Amusia, A. S. Baltenkov, and L. V. Chernysheva, JETP Lett. **111**, 18 (2020).

[64] J. D. Bjorken and S. D. Drell, *Relativistic Quantum Mechanics* (McGraw-Hill, New York, 1964).

[65] C. F. Fischer and K. M. S. Saxena, Phys. Rev. A **9**, 1498 (1974).

[66] B. H. Bransden and C. J. Joachain, *Physics of Atoms and Molecules* (Pearson Education, India, 2003).

[67] S. K. Lin, J. Chem. Inf. Comput. Sci. **36**, 367 (1996).

[68] P. V. Giaquinta and G. Giunta, Physica A **187**, 145 (1992).

[69] W. Ebeling and T. Pöschel, Europhys. Lett. **26**, 241 (1994).

[70] C. H. Lin and Y. K. Ho, Chem. Phys. Lett. **633**, 261 (2015).

[71] K. D. Sen, J. Chem. Phys. **123**, 074110 (2005).

[72] T. Schedel-Niedrig, M. C. Böhm, H. Werner, J. Schulte, and R. Schlögl, Phys. Rev. B **55**, 13542 (1997).

[73] M. E. Madjet, T. Renger, D. E. Hopper, M. A. McCune, H. S. Chakraborty, J.-M. Rost, and S. T. Manson, Phys. Rev. A **81**, 013202 (2010).

[74] N. L. Guevara, R. P. Sagar, and R. O. Esquivel, Phys. Rev. A **67**, 012507 (2003).

[75] A. S. Hyman, S. I. Yaniger, and J. F. Liebman, Int. J. Quantum Chem. **XIV**, 757 (1978).

[76] R. F. Stewart, E. R. Davidson, and W. T. Simpson, J. Chem. Phys. **42**, 3175 (1965).

[77] H. M. Lee, M. M. Olmstead, T. Suetsuna, H. Shimotani, N. Dragoe, R. J. Cross, K. Kitazawa, and A. L. Balch, Chem. Commun. **46**, 1352 (2002).